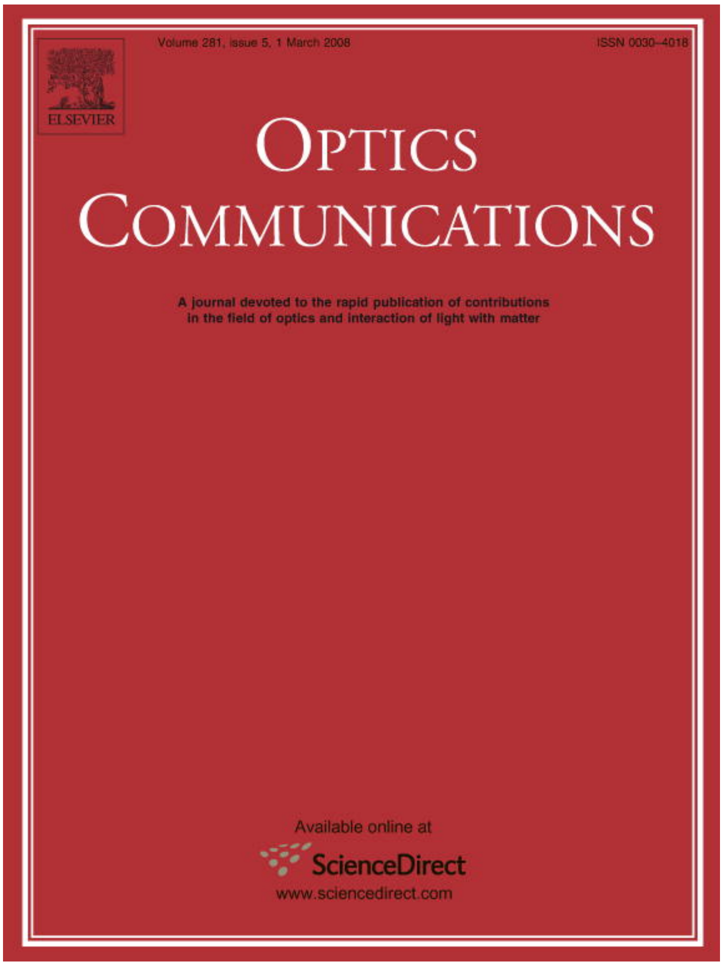
Volume 281, issue 5, 1 March 2008
ISSN 0030-4018
ELSEVIER
OPTICS COMMUNICATIONS
A journal devoted to the rapid publication of contributions in the field of optics and interaction of light with matter
Available online at
ScienceDirect
www.sciencedirect.com

Available online at www.sciencedirect.com
ScienceDirect
Optics Communications 281 (2008) 953–957
OPTICS COMMUNICATIONS
www.elsevier.com/locate/optcom

All-optical super resolved and extended depth of focus imaging with random pinhole array aperture

Zeev Zalevsky [a], Javier García [b,*]

[a] *School of Engineering, Bar-Ilan University, Ramat-Gan 52900, Israel*
[b] *Departamento de Óptica, Universitat de Valencia, c/Dr. Moliner, 50, 46100 Burjassot, Spain*

Received 15 May 2007; accepted 15 October 2007

Abstract

In this paper, we present a novel approach which allows combining super resolved imaging with extended depth of focus while the result is obtained by all-optical means and no digital processing is required. The presented approach for the super resolved imaging includes attaching a random pinhole array plate to the aperture plane of the imaging system. The energetic efficiency of the system is high and it is much larger than an imaging through a single pinhole which also has extended depth of focus. The super resolving result is obtained by mechanic scanning of the aperture plane with the random plate.

1. Introduction

Super resolution is a widely investigated field in which spatial degrees of freedom are recovered by sacrificing other dimensions as polarization, wavelength and time [1–5]. Depth of focus is very important feature which is in a way resembles longitudinal super resolution. The meaning of it is the longitudinal range of positions at which an object can sharply be imaged using an imaging module [6–11]. A pinhole camera allows capturing images with infinitely extended depth of focus [12]. Since instead of a lens a pinhole is placed, this imaging system is lensless. However, such a camera has no resolution and the energetic efficiency is very low. This is due to the fact that the point spread function (1/resolution) is proportional to $\lambda d_i/D$ (where λ is the wavelength, D the aperture of the lens and d_i is the distance between the lens and the detector), the depth of focus to $\lambda(d_i/D)^2$ and the energetic efficiency to D^2. Thus, a pinhole that has small D has low resolution (large point spread function) large depth of focus and low energetic efficiency. A different approach for enlarging the depth of field consists on using an annular aperture. This aperture produces an optical transfer function (OTF) which consists on a large low amplitude plateau with a central spike at zero frequency. This OTF remains essentially constant against focus changes in the limit case where the width of the annulus tends to zero [13,14].

In this paper, we propose to use the extended depth of focus advantage that the lensless imager (a pinhole camera) has but yet to improve its resolution and energetic efficiency. The basic idea is simple. Let us use instead of one pinhole a set of many pinholes randomly distributed along the lens' aperture plane. The aperture plane can be composed out of holes (transmission/blocking function) or even a random phase distribution as in a *diffuser*. We will coin this filter that is placed in the aperture plane of the imaging lens as: *random plate*. The random distribution is such that at least half of the energy passes through (for the case it is composed out of holes). Since the spatial distribution is random its autocorrelation (corresponding to optical transfer function) is still similar to a delta function as that of a single pinhole. Thus, this enables us to have simultaneously energetic efficiency (of half instead of almost a zero in the pinhole camera case) and extended

* Corresponding author.
E-mail address: javier.garcia.monreal@uv.es (J. García).

0030-4018/$ - see front matter © 2007 Elsevier B.V. All rights reserved.
doi:10.1016/j.optcom.2007.10.065

depth of focus. However, the resolution is still, as for a pinhole camera, low. In order to improve resolution we use a proper replication of the amplitude (including the random mask) at the system aperture that permits the sampling of a single frequency of the image. Then we scan the aperture plane with the random plate and time integrate the intensity at the detector. As we are about to show, this scanning generates super resolving imaging and allows the establishment of simultaneously extended depth of focus, high spatial resolution and energetically efficient image. The super resolution is obtained in an all-optical manner (no image processing is required). The super resolution applied in the described approach can be categorized as time multiplexing.

Section 2 describes the operation principle and its optical configuration. Numerical testing is presented in Section 3. The paper is concluded in Section 4.

2. Operation principle

Under paraxial approximation, the defocus can be modeled as a quadratic phase factor over the pupil of the optical system [12]

$$\widehat{P}(x,y) = P(x,y)\exp[\mathrm{i}W_m(x^2+y^2)] \tag{1}$$

where P represent the pupil function, $\widehat{P}$ stands for the generalized complex pupil function and W_m is a coefficient expressing the amount of defocusing. The OTF is given by the normalized autocorrelation of the generalized pupil function. In this autocorrelation approach, the low contrast in a defocus system derives from the poor overlapping between the generalized pupil and a shifted replica of it. The purpose of the following derivation is to achieve an OTF that will provide a high value for a given frequency.

For achieving this goal we propose the conceptual setup that is depicted in Fig. 1a. We recall the generalized pupil in Eq. (1) comes from the derivation of the impulse response of the system; for a delta input the pupil results

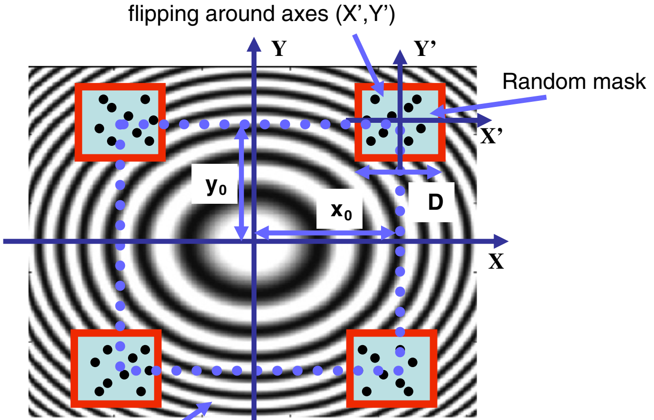

Fig. 1. Schematic illustration of the aperture plane.

illuminated with a spherical phase factor. We assume that there is an element located at position (x_0, y_0), in the upper right quadrant of the aperture, consisting of the random plate. By some optical mechanism that we will explain shortly we generate flipping that may have 4- or 2-folds. For instance instead of the original distribution $g(x', y')$ we will generate spatial distribution of $0.5\times[g(x', y')+g(-x', -y')]$ while $g(x', y')$ is the multiplication of the quadratic phase (spherical wave front) with the random plate transmission function (see Fig. 1). Using similar optical mechanism that generated 4-folds symmetry in the (x', y') coordinates set, we will generate 4-fold symmetry in the (x, y) coordinates set (see Fig. 1). Therefore, the distribution of $0.5\times[g(x',y')+g(-x', -y')]$ is replicated 4 times around the origin in the (x, y) coordinates. The aim of this mirroring is to maintain the desired orthogonality as is to be explained next. The resulting distribution has symmetry around the origin but also has a partial replication when shifted by $(2x_0, 2y_0)$.

Let us now write the explicit mathematical expressions describing the four terms we have in the aperture plane. First, following the notations presented in Fig. 1 we may write that

$$x' = x - x_0 \quad y' = y - y_0 \tag{2}$$

Denoting by $E(x', y')$ the field generated just after the upper right random plate when it is illuminated with a spherical wave front (due to defocusing) function of $\exp[\mathrm{i}W_m(x^2+y^2)]$

$$E(x',y') = \frac{m(x',y')}{2}\cdot\exp\left(\mathrm{i}W_m((x'+x_0)^2+(y'+y_0)^2)\right) + \frac{m(-x',-y')}{2}\cdot\exp\left(\mathrm{i}W_m((-x'+x_0)^2+(-y'+y_0)^2)\right) \tag{3}$$

$m(x', y')$ is the random plate. The two terms are due to the 2-folds symmetry we have mentioned first. We assume that the random plate itself is also symmetric, i.e., $m(x', y') = m(-x', -y')$ and thus one obtains

$$E(x',y') = m(x',y')\cos(2W_m(x'x_0+y'y_0)) \times \exp\left(\mathrm{i}W_m(x'^2+x_0^2+y'^2+y_0^2)\right) \tag{4}$$

Following the effect of the two perpendicular mirrors (the 4 replications) one may obtain the total output

$$E_{\mathrm{tot}}(x,y) = E(x,y)+E(-x,-y)+E(-x,y)+E(x,-y) \tag{5}$$

The autocorrelation of the total field at the aperture, as given by Eq. (5) gives the final OTF. Note that this fact can be expressed as the calculation of the impulse response, as the Fourier transform of the field at the aperture, intensity conversion and then inverse Fourier transform.

Since $m(x', y')$ is a random function, its autocorrelation can be approximated by a delta function

$$\int_{-\infty}^{\infty}\int_{-\infty}^{\infty} m(x',y')m^*(x'-x'',y'-y'')\,\mathrm{d}x'\,\mathrm{d}y' = \delta(x'',y'') \tag{6}$$

and since the coefficients or the rest of the terms appearing in Eq. (4) [in addition to $m(x', y')$] are also symmetric around the axes (x', y') (i.e., around the center of the random plate) they will even reinforce the sharpness of the delta function in the autocorrelation operation of E_{tot} when cross-terms as $E(-x, -y)$ and $E(x, y)$, for instance, are correlated. Thus, the overall result obtained after using the relation of Eq. (5) in the autocorrelation expression of Eq. (4) yields

$$\int_{-\infty}^{\infty}\int_{-\infty}^{\infty} E_{\text{tot}}(x,y)E^{*}_{\text{tot}}(x-x'',y-y'')\,\mathrm{d}x\,\mathrm{d}y$$
$$= \delta(x'',y'') + \delta(x''-x_0,y''-y_0) + \delta(x''+x_0,y''+y_0) + \delta(x''-x_0,y''+y_0) + \delta(x''+x_0,y''-y_0) \tag{7}$$

This result is obtained by autocorrelating Eq. (5) and substituting it into Eq. (4) while assuming the relation of Eq. (6). In abstract, aside of the DC term, the OTF permits the recording of a given spatial frequency and its symmetric terms (as given by the element position (x_0, y_0)) and, most important, independently of the amount of defocus. The folding of the complex distribution at the pupil plane allows the setting of the central frequency that will pass the system while the random plate makes a narrow band-pass around the selected frequency.

Finally, we assume that there is a mechanical scan shift of the element that allows the scan of the (x_0, y_0) position. The scanning will fill the OTF of the system is a time sequential manner. Note that this is a very interesting result that will allow us to achieve our goal: super resolution and mostly extended depth of focus while maintaining high energetic efficiency. The spatial coordinates of the field in the aperture plane as appearing in Eqs. (5) and (7) can be related to spatial frequency by: $x = \lambda d_i v_x$ and $y = \lambda d_i v_y$ where λ is the wavelength, d_i is the distance between the aperture plane and the detector and v_x, v_y are the spatial frequencies in the horizontal and the vertical axes, respectively [12].

Now let us discuss the optical mechanism for practical realization of the 4- or 2-folds symmetry. In order to have a practical solution we suggest the configuration described in Fig. 2. The upper part of the figure shows the 3D structure of the optical setup for 4-folds symmetry while the lower part shows its 2D cross-section which includes also ray tracing. The simplified description is for the imaging lens of our imager. The description is for the elements positioned between the entrance and the exit pupils of the imaging lens. At the entrance pupil of the imaging lens we place the random mask. Attached to the lenses of the setup a spatial light modulator (SLM1) is attached. This SLM includes a realization of a diffractive lens with additional optical power. This diffractive element has two diffraction orders of one and zero. The zero diffraction order has no optical power and therefore the fixed lenses having the focal length of F perform an imaging with magnification of -1 between the entrance and the exit pupils (inverted image). For the first diffraction order to the element displayed on SLM1 is a lens with focal length of F.

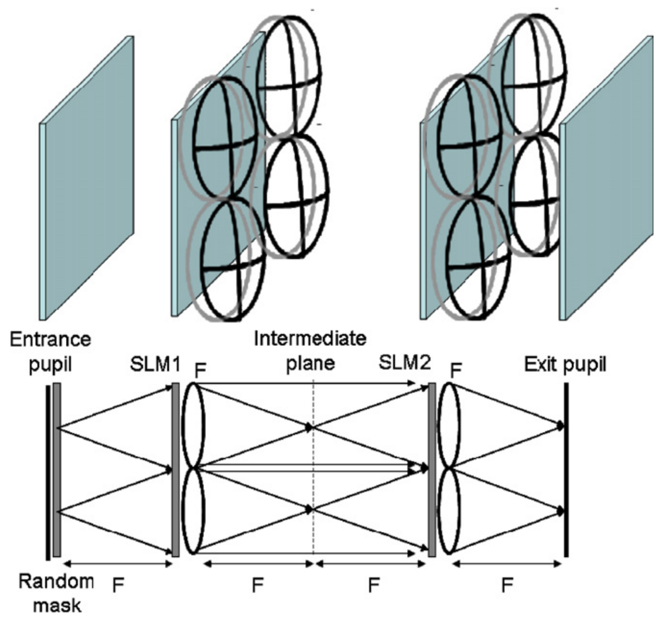

Fig. 2. Practical realization of the proposed concept. Description of the elements positioned between the entrance/exit pupils of the imaging lens.

The total focal length of two attached lenses each having focal length of F equals to $F/2$ and therefore an imaging of the entrance pupil (and the random mask that is placed there) is obtained in the intermediate plane. SLM2 displays a diffractive element equal to the one of SLM1 and therefore additional imaging is performed between the intermediate plane and the exit pupil. Therefore, since in regular imaging the image is inverted, in double imaging the image is the same (i.e., the magnification is 1) and if we denote by $g(x, y)$ the multiplication between the random mask placed in the entrance pupil and the quadratic phase created there due to defocusing, at the exit pupil one obtains $g(x, y) + g(-x, -y)$. By adding a linear phase factor [i.e., $\exp(2\pi i\alpha_x(t)x + 2\pi i\alpha_y(t)y)$] to the function displayed in SLM1 and SLM2 and varying its slope with time (i.e., $\alpha_x(t)$ and $\alpha_y(t)$ vary with time) will generate the spatial scanning of the random aperture versus time. This will happen since the SLMs are attached to the imaging lenses and therefore their effect is as operating over the Fourier plane (adding linear phase in the Fourier plane will shift the image).

Note that the configuration proposed in Fig. 2 includes four lenses. This is needed in order to create the 4-folded symmetry around the optical axis of the entire imagining system, as explained in Eq. (4). Obviously, the grating functions that are displayed on the SLM and that generate the spatial scanning are flipped between the four regions (each region is corresponding to each one of the four lenses). This is needed in order to have the 4-folded flipping symmetry between the four terms of Eq. (4).

Note also that the same setup can be realized in reflection and then half of the elements are spared. In this configuration the reflection mirror is placed in the intermediate plane of the imaging lens of Fig. 2.

3. Numerical testing

The system of Fig. 2 was simulated and the results are presented in Figs. 3–5. The amount of defocusing is measured as the maximal phase obtained at the edges of the aperture. In our case

$$\psi = \frac{W_m D^2}{4} = \frac{\pi D^2}{4\lambda}\left(\frac{1}{d_i} + \frac{1}{d_o} - \frac{1}{F}\right) \tag{8}$$

where d_o and d_i are the distances from the object or the image to the aperture plane, respectively. D is the diameter of the aperture. W_m is a coefficient that is related to the focusing relation as seen from the right part of the equation. F is the *effective* focal length of the imaging system to which we attend to match the performance of our solution. In the simulations the defocusing distortion was simulated for a range of values of the parameter ψ. The range was from zero (no spherical wave is generated on the aperture plane) and up to large numbers as 25.

In Fig. 3, we present the reconstruction of a script image. In Fig. 3a, we present the results obtained for $\psi = 10$ while the proposed approach is applied. In Fig. 3b, one may see the result obtained for the same ψ and without applying the suggested approach. In Fig. 3c and d, one may see the results obtained in focus ($\psi = 0$) with and without the suggested approach, respectively. In the simulations we assumed, as in the mathematical deriva-

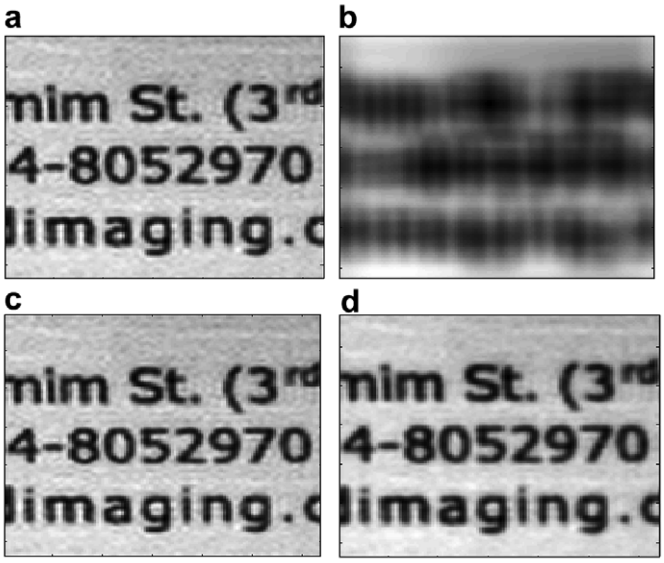

Fig. 3. Simulated results for script. (a) The result obtained for $\psi = 10$ and when the proposed approach is applied. (b) The result obtained for the same ψ and without applying the suggested approach. (c) The results obtained in focus ($\psi = 0$) with the suggested approach. (d) The results obtained in focus ($\psi = 0$) without the suggested approach.

Fig. 5. As in Fig. 3 but for a face object.

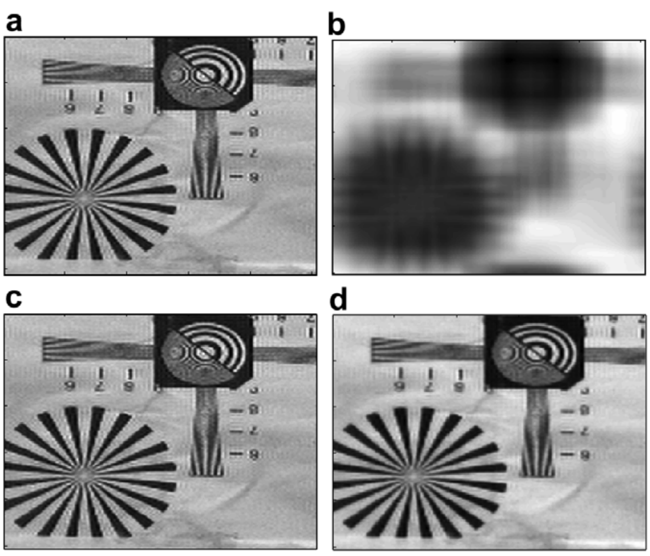

Fig. 4. As in Fig. 3 but for resolution target.

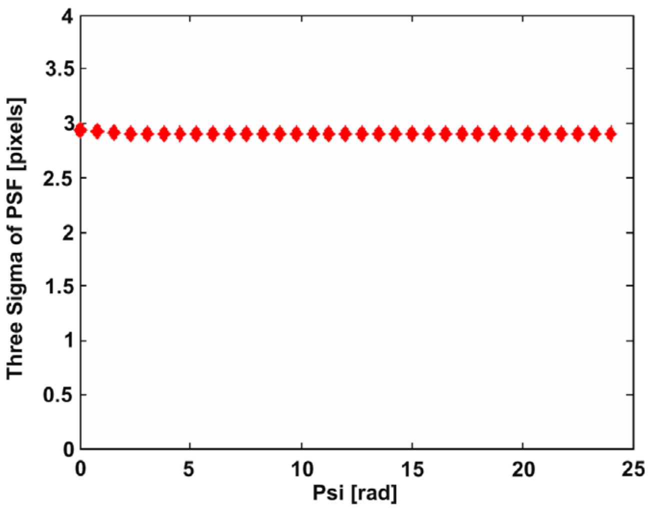

Fig. 6. The width of three standard deviation of a point spread function versus the amount of defocusing (the value of ψ).

tion, that the random plate is attached to the aperture plane of an imaging lens and thus a Fourier relation exists between this plane and the detector. This assumption is correct for any imaging system as well as for lensless imager, such as a pinhole camera, if the size of the pinhole and the distance of the aperture plane from the detector justify the far field approximation. Figs. 4 and 5 are the same as Fig. 3 but for resolution target and face object used as an input object, respectively. Note that the results presented in Figs. 3–5 are all-optical and no image processing was applied to further enhance them.

Fig. 6 presents the width of three standard deviations of an intensity point spread function obtained in the image plane versus the amount of defocusing (the value of ψ). One may see that even for very strong defocusing of $\psi = 25$ the standard deviation of the spatial point spread function of the intensity remains only *1 pixel* in units of $\lambda d_i/D$.

4. Conclusions

In this paper, we have proposed an approach in which a random plate and a folding system is attached to the aperture plane of an imaging system. The plate is shifted around the aperture plane while light is being integrated by the detector. The obtained result is super resolved image with almost infinite depth of focus and high energetic efficiency of around half (for the case the random plate is composed out of holes) for every image capturing (in comparison to a pinhole camera where a lensless imaging provides infinite depth of focus as well but zero energetic efficiency and very low spatial resolution).

Acknowledgements

This work was supported by FEDER funds and the Spanish Ministerio de Educación y Ciencia under the Project FIS2007-60626.

References

[1] Z. Zalevsky, D. Mendlovic, A.W. Lohmann, Progr. Opt. XL (1999) (Chapter 4).
[2] Z. Zalevsky, D. Mendlovic, Optical Super Resolution, Springer, 2002.
[3] W. Lukosz, JOSA 56 (1966) 1463;
W. Lukosz, J. Opt. Soc. Am. 56 (1966) 1463.
[4] A.I. Kartashev, Opt. Spectrosc. (USSR) 9 (1960) 204.
[5] W. Gartner, A.W. Lohmann, Z. Phys. 174 (1963) 18.
[6] E.R. Dowski Jr., W. Thomas Cathey, Appl. Opt. 34 (1995) 1859.
[7] J. van der Gracht, E.R. Dowski Jr., M.G. Taylor, D.M. Deaver, Opt. Lett. 21 (1996) 919.
[8] J.O. Castaneda, E. Tepichin, A. Diaz, Appl. Opt. 28 (1989) 2666.
[9] E. Ben-Eliezer, Z. Zalevsky, E. Marom, N. Konforti, J. Opt. A: Pure Appl. Opt. 5 (2003) 164.
[10] Z. Zalevsky, A. Shemer, A. Zlotnik, E.B. Eliezer, E. Marom, Opt. Exp. 14 (2006) 2631.
[11] A. Sauceda, J. Ojeda-Castañeda, Opt. Lett. 29 (2004) 560.
[12] J.W. Goodman, Introduction to Fourier Optics, McGraw-Hill, New York, 1996.
[13] J.T. McCrickerd, Appl. Opt. 10 (1971) 2226.
[14] C.J.R. Sheppard, A. Choudhury, Appl. Opt. 43 (2004) 4322.